Materials Today • Volume xxx, Number xx • xxxx 2018 RESEARCH

ELSEVIER

Ultrabright fluorescent cellulose acetate nanoparticles for imaging tumors through systemic and topical applications

Berney Peng [1,†,‖], Mohammad Almeqdadi [2,3,4,‖], Fabrice Laroche [5,6], Shajesh Palantavida [7,‡], Maxim Dokukin [7,¶], Jatin Roper [3,4], Omer H. Yilmaz [3], Hui Feng [5,6], Igor Sokolov [1,7,8,*]

[1] Department of Biomedical Engineering, Tufts University, Medford, MA, USA
[2] Department of Medicine, St. Elizabeth's Medical Center, Boston, MA, USA
[3] The David H. Koch Institute for Integrative Cancer Research at MIT, Cambridge, MA, USA
[4] Department of Medicine, Tufts Medical Center, Boston, MA, USA
[5] Department of Pharmacology and Experimental Therapeutics, Boston University School of Medicine, Boston, MA, USA
[6] Department of Medicine, Boston University School of Medicine, Boston, MA, USA
[7] Department of Mechanical Engineering, Tufts University, Medford, MA, USA
[8] Department of Physics, Tufts University, Medford, MA, USA

Cellulose acetate (CA), viscose, or artificial silk are biocompatible human-benign derivatives of cellulose, one of the most abundant biopolymers on earth. While various optical materials have been developed from CA, optical CA nanomaterials are nonexistent. Here we report on the assembly of a new family of extremely bright fluorescent CA nanoparticles (CA-dots), which are fully suitable for in vivo imaging/targeting applications. CA-dots can encapsulate a variety of molecular fluorophores. Using various commercially available fluorophores, we demonstrate that the fluorescence of CA-dots can be tuned within the entire UV–VIS-NIR spectrum. We also demonstrate excellent specific targeting of tumors in vivo, when injected in zebrafish (xenograft model of human cervical epithelial cancer), and unusually strong exvivo topical labeling of colon cancer in mice utilizing CA folate-functionalized nanoparticles.

Introduction

Fluorescent nanoparticles are becoming increasingly popular in biomedical detection and imaging [1,2]. Compared to molecular fluorophores, fluorescent nanoparticles are typically brighter and more photostable. They can also be functionalized with more than one sensing molecule and utilized for the tagging and tracing of specific molecules, cells, tissues [3–8]. Brighter fluorescence facilitates higher signal-to-noise ratio, more sensitive labeling, typically lower limit of detection, etc. The most developed (and commercially available) bright fluorescent nanoparticles are quantum dots (QDs) [9–12]. Although excellent in many aspects, they still exhibit a number of problems, including potential toxicity, significant fractions of non-fluorescent QDs, and blinking, etc. [13]. Polymer dots [14–17], an organic version of QDs, are promising bright particles which are still under development and have a limited number of available semiconductor polymers. Biodegradation and long-term toxicity of polymer dots have yet to be determined.

Here we report on ultrabright fluorescent nanoparticles (brighter than QDs and sometimes polymer dots of similar spectrum [18]) and that are made of one of the most biocompatible,

* Corresponding author.
E-mail address: Sokolov, I. (Igor.Sokolov@tufts.edu)
† Address before 2017: NanoScience Solutions, LLC, Woburn, MA, USA.
‡ Present address: Center for Nano and Material Sciences, Jain University, Jakkasandra, Kanakapura, Karnataka 562112, India.
¶ Present address: National Research Nuclear University MEPhI, Kashirskoe sh. 31, Moscow 115409 Russia.
‖ Equal contribution.

 https://doi.org/10.1016/j.mattod.2018.11.001

Please cite this article in press as: B. Peng et al., Materials Today (2018), https://doi.org/10.1016/j.mattod.2018.11.001

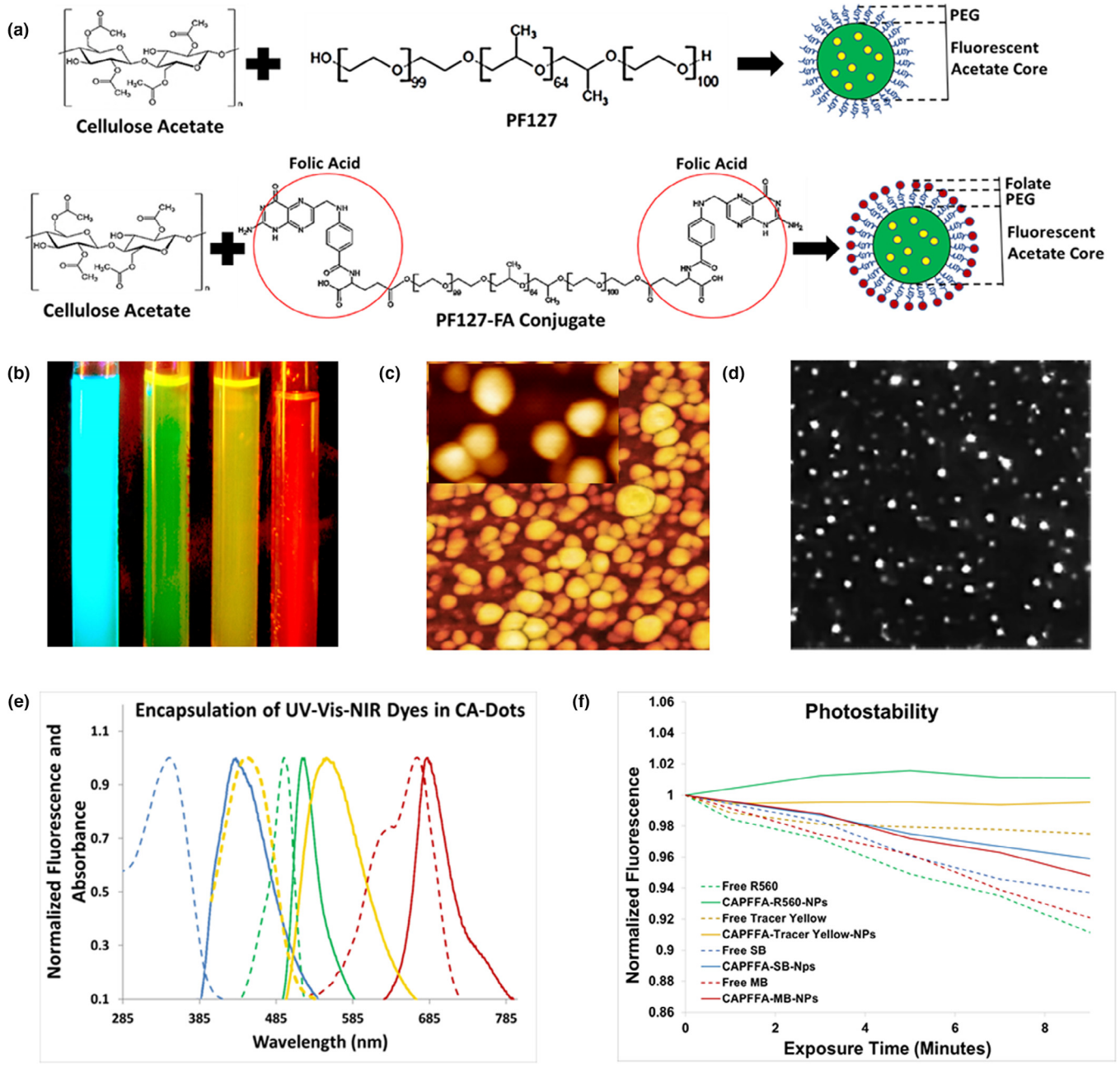

FIGURE 1

Assembly of CA-dots and their basic properties. (a) Schematics of the assembly. A physical mix of cellulose acetate dissolved in an organic solvent and pluronic acid F127 dissolved in an aqueous phase to produce PEG-coated CA-dots; folate functionalized CA-dots are assembled in a similar way by substituting F127 "module" with FA-F127 conjugate. (b) Fluorescent image of four tubes with CA-dots containing encapsulated Stilbene 420 (blue), Rhodamine 560 (green), Tracer Yellow (yellow), and Methylene Blue (red/NIR); fluorescence of blue, green, and yellow CA-dots were excited with UV flashlight, and the NIR dye with 660 nm red laser. The image was taken with Fuji Pro camera with extended NIR sensitivity. (c) $1 \times 1\ \mu m^2$ AFM image of CA nanoparticle (CA-SB-PEG-FA); insert is $170 \times 270\ nm^2$ image showing about spherical geometry of the particles; (d) $25 \times 25\ \mu m^2$ fluorescent image of single CA-dots near the surface of a glass slide; (e) absorbance and fluorescence spectra of CA-dots with encapsulated different fluorescent dyes: blue (ex/em: 365 nm/420 nm; Stilbene 420), green (ex/em: 495 nm /530 nm; Rhodamine 560), yellow (ex/em: 450 nm /560 nm; Tracer Yellow), and red/NIR (ex/em: 665 nm/680 nm; Methylene Blue) maxima of fluorescent intensity. (e) photostability of the obtained particles and the corresponding free dye; a short-time exposure is shown in which photodegradation kinetics are comparable (relative beaching < 10%).

non-toxic human benign materials, cellulose acetate (CA), viscose, or artificial silk. There is an enormous wealth of knowledge developed during the last century about production, doping, and functionalization of cellulose-based materials on a massive industrial scale. Cellulose acetate has been used in biomedical areas in drug packaging, antimicrobial composites, controlled drug release, wound dressing, bone repairing, and tissue engineering [19], as a membrane support for various sensors [20,21]. Various optical materials have also been developed based on CA [22,23]. Any attempts to make fluorescent CA

Please cite this article in press as: B. Peng et al., Materials Today (2018), https://doi.org/10.1016/j.mattod.2018.11.001

nanoparticles resulted in the particle size of 100–500 nm and larger [24,25]. This large size is not suitable for in-vivo applications because such particles are cleared by organisms excessively fast [26]. As was shown, an optimum size of particles of 20–90 nm is preferable for such applications [27]. In vivo applications of CA nanoparticles are rather attractive because of complete human biocompatibility, low cost, and a wealth of knowledge of CA modification.

In this work, we specifically present the composite assembly of ultrabright fluorescent CA nanoparticles of 50–90 nm in size (CA-dots). Particles become fluorescent through incorporating existing fluorescent dyes into the CA nanoparticle matrix. Besides the simplicity of such synthesis, it allows coverage of the entire optical spectrum, from UV–Vis to NIR. We found robust functionalization of the particles with small biomolecules (for example, folates, a ligand targeting the majority of epithelial cancers [28]) and protective polyethylene glycol (PEG) molecules, the layer needed to decrease nonspecific interactions of the particles with the surrounding in vivo. We establish that such particles are capable of efficient detecting and targeting even small tumors in zebrafish in vivo. Moreover, CA-dots exhibit unusually fast and strong labeling of colon tumors in the mouse colon when applied just topically.

Results and discussion

Assembly of CA-dots with fluorescent spectra in the entire UV–VIS-NIR range

A modified nanoprecipitation [24] approach was employed to manufacture particles in solvents of varying polarity, which facilitated the supramolecular assembly of CA and co-assembled with a guest polymer such as Pluronic F-127, a nonionic, amphiphilic polymer possessing polyethylene glycol (PEG) blocks. In contrast to other nanoprecipitation approaches utilizing cellulose, the described method produces particles of (a) smaller sizes, (b) high fluorescent brightness that covers the entire spectrum from UV–Vis to NIR, and (c) surface functionalization with PEG groups and/or biologically relevant molecules. The use of PEG groups not only allows attaining smaller sizes but also enhances colloidal stability and makes the particles suitable for in vivo applications, an important feature demonstrated in this work.

To functionalize CA-dots, we have developed a facile and modular two-stage one-pot synthesis by first conjugating a biomolecule of interest to the secondary co-assembling polymer, and subsequently, performing the supramolecular assembly step. Polymeric guests participate in the formation of hydrophobic and hydrophilic nanodomains during the supramolecular assembly process. Water drives precipitation of CA dissolved in the organic medium into the aqueous environment; precipitation-catalyzed particle nucleation occurs at the water-organic interface [29,30]. Hydrophobic interactions dominate throughout this process, and the flexibility and the amphiphilic nature of the CA backbone enable hydrophobic acetate groups to preferentially assemble toward the core of the particle while hydrophilic hydroxyls remain outward [31]. Because polymers and block copolymers like PF127 also possess hydrophilic and hydrophobic moieties, we hypothesized that such polymers will also diffuse into CA-nucleating regions. The formation of a hydrophobic core preferentially concentrates the polymer guest toward the surface, eventually becoming trapped during phase separation [25]. This results in the desired surface functionalities. Here we demonstrate this approach by functionalizing CA-dots with folate molecules (Fig. 1a, and Fig. 1 of Ref. 32), which made the particles specific to the majority of epithelial cancers [28]. Larger molecules, like antibodies can be attached to CA-dots in a more traditional way through, for example, utilizing amine-reactive crosslinker reactive groups like N-hydroxysuccinimide esters (NHS esters) and its derivatives [33].

To demonstrate the ability to assemble particles spanning the entire UV–VIS-NIR fluorescent spectrum, we chose to encapsulate four commercial dyes: Stilbene 420, Rhodamine 560, Tracer Yellow, and Methylene Blue. One can see that the fluorescent spectra of the obtained particles cover the entire spectrum (Fig. 1b,e), with the maximum absorbance ranging from 350 to 665 nm and the maximum emission from 445 to 680 nm (Table 1). Each particle name consists of three parts: CA-Color-Coating molecules (CA stands for cellulose acetate). For example, CA-GREEN-PEG means cellulose acetate with encapsulated Rhodamine 560 (green) dye, coated with PEG molecules. CA-GREEN-PEG-FA means the same particle with additionally added folic acid molecules coating such particles.

TABLE 1

Physical parameters of synthesized particles: size, the parameter characterizing poly-dispersity in size (PDI), excitation/emission fluorescent maxima, fluorescent brightness, the zeta potential, and the number of folate molecules per single nanoparticle. Four commercially available dyes were used to demonstrate the assembly of CA-dots fluorescent in the entire UV–VIS-NIR spectrum. Stilbene 420 (blue), Rhodamine 560 (green), Tracer Yellow (yellow), Methylene Blue (red/NIR) were used for encapsulation. Data for particles covered with PEG and PEG + folate are shown. Brightness relative to quantum dots was calculated for ^{1}QD450 [40] (brightness 1×10^5 M^{-1} cm^{-1}), ^{2}QD525 [41] (brightness 1.3×10^5 M^{-1} cm^{-1}), ^{3}QD585 [41] (brightness 3.05×10^5 M^{-1} cm^{-1}), QD705 [42] (brightness 1.2×10^6 M^{-1} cm^{-1}).

CA-dot	Size, Mn (nm)	PDI	Ex/Em (nm/nm)	Brightness (MBTU)/M·cm^{-1}	Brightness relative to QD (times)	Zeta-Potential (mV)	Folates per particle
CA-SB-PEG	61	0.22	400/445	$89 \pm 4/(5.8 \pm 0.3) \times 10^6$	58[1]	−8.0 ± 1	N/A
CA-SB-PEG-FA	50	0.17	400/445	$529 \pm 42/(3.4 \pm 0.3) \times 10^7$	340[1]	−11 ± 1	870 ± 220
CA-GREEN-PEG	77	0.13	495/525	$870 \pm 71/(6.4 \pm 0.5) \times 10^7$	640[2]	−17 ± 2	N/A
CA-GREEN-PEG-FA	68	0.14	495/525	$781 \pm 49/(5.8 \pm 0.4) \times 10^7$	580[2]	−15 ± 3	910 ± 200
CA-YEL-PEG	60	0.15	450/560	$159 \pm 13/(4.3 \pm 04) \times 10^6$	43[3]	−3 ± 2	N/A
CA-YEL-PEG-FA	87	0.11	450/560	$649 \pm 92/(1.8 \pm 0.3) \times 10^7$	180[3]	−7 ± 1	1110 ± 180
CA-RED/NIR-PEG	77	0.17	665/680	$2554 \pm 268/(1.3 \pm 0.1) \times 10^8$	1300[4]	−19 ± 1	N/A
CA-RED/NIR-PEG-FA	63	0.20	665/680	$318 \pm 38/(1.6 \pm 0.2) \times 10^7$	160[4]	−12 ± 2	930 ± 290

Please cite this article in press as: B. Peng et al., Materials Today (2018), https://doi.org/10.1016/j.mattod.2018.11.001

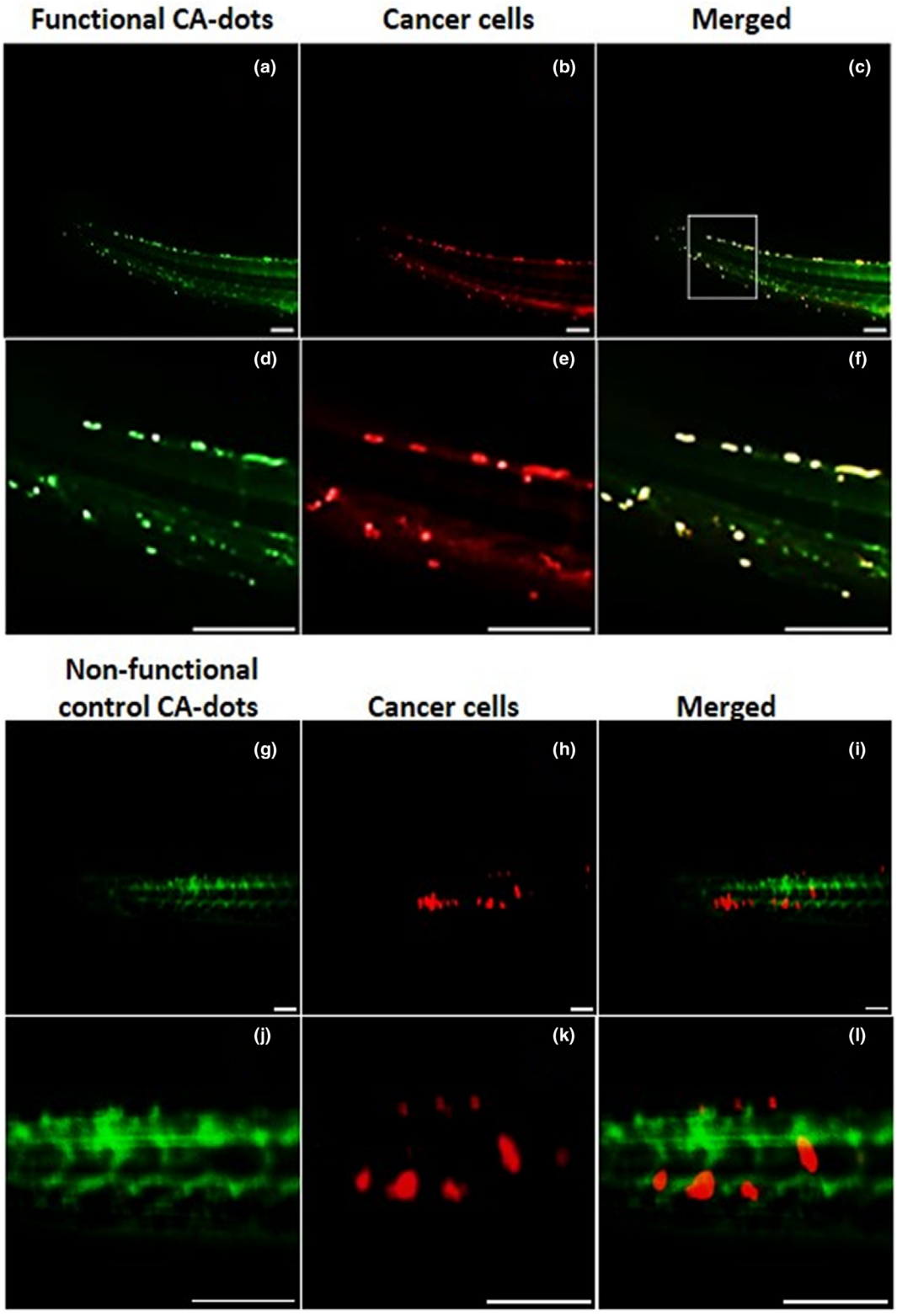

FIGURE 2

Demonstration of targeting performance of HeLa xenographic tumors in zebrafish with PEG-*folate* functionalized CA-dots versus PEGylated CA-dots (control). Colocalization is clearly observed 30 (Fig. 6 of Ref. 32) and 50 min (shown here) following the IV injection. Blue fluorescent CA-dots are shown in green (for better visualization) while cancer cells expressing RFP are shown in red (equal mixture of red and green gives yellow). Panel (a–c) shows fluorescence of the full zebrafish tail 50 min after administering folate-functionalized CA-dots. Panels (d–f) are zoomed sections to demonstrate clear evidence of tumor targeting. Panel (g-f) shows fluorescence of the full zebrafish tail with PEGylated control CA-dots 50 min after administration. Panels (j-k) are zoomed sections demonstrating less successful cancer targeting. Scale bar is 100 μm.

Please cite this article in press as: B. Peng et al., Materials Today (2018), https://doi.org/10.1016/j.mattod.2018.11.001

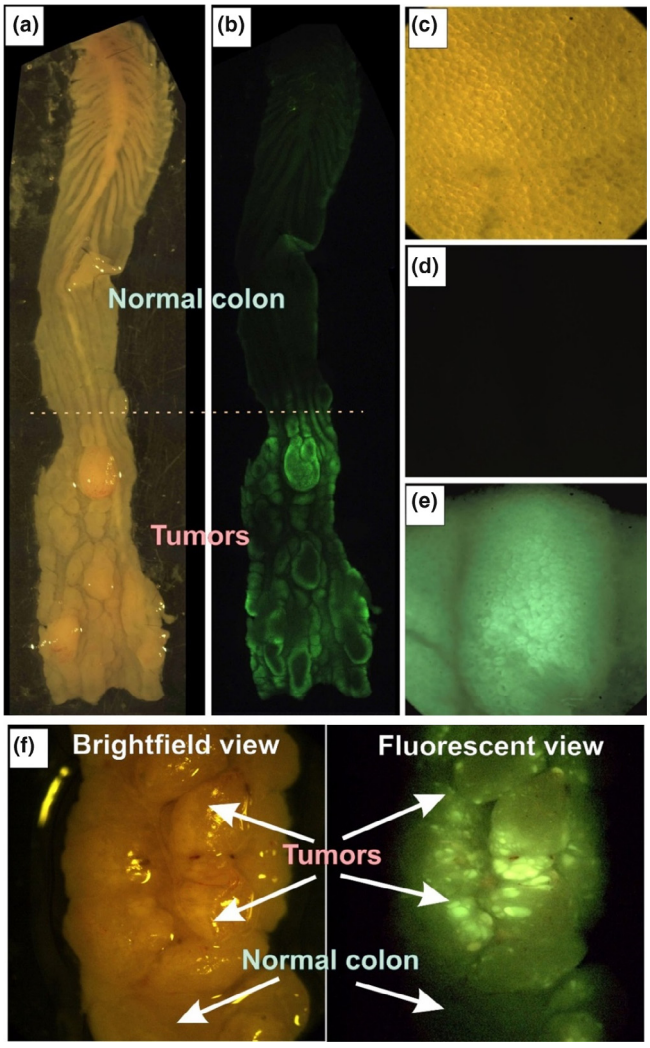

FIGURE 3

Ex vivo VillinCreERT2-Apcfl/fl mouse colon with developed colorectal cancer labeled using folate functionalized green CA-dots (CA-GREEN-PEG-FA). Tumor areas are easily identifiable in the bright field images of colon shown in panels (a) and (f). Fluorescent images of the colons (b), (e) and (f) show a clear colocalization of green fluorescence and tumors. Normal parts of the colons do not show any noticeable fluorescence (b), (d), (f). The latitudinal size of the open colon is ~5 mm. Images (c–e) are 1×1 mm^2. High heterogeneity of labeled tumor structure is clearly seen in panel (f).

Physical characteristics of CA-dots

Physical characteristics of CA-dots (Table 1) indicate that we can obtain nanoparticles within the average size of 50–90-nm range (measured with dynamic light scattering, DLS) with good monodispersity (PDI index). The particles size varies with dye and surface functionalization. CA-dots have approximately spherical morphology as seen in the AFM images (Fig. 1c). Accounting for tip convolution, AFM images of single particles had the article diameters similar to the DLS size (for example, 40–50 nm in AFM versus 50–60-nm hydrodynamic size in DLS).

The fluorescent brightness of CA-dots is found (Table 1) using the brightness measurements relative to a molecule of the known molecular fluorophore. It is calculated in so-called MESF units (Molecules of Equivalent Soluble Fluorophore; the units used in flow cytometry [11,34–37]). We also present these values in terms of another definition of brightness, as a multiplication of the quantum yield ϕ and the extinction coefficient $\varepsilon(\lambda)$ ($M^{-1}\,cm^{-1}$ units). The latter is a convenient way to compare the brightness of the synthesized CA-dots with other fluorescent particles, for example, quantum dots. One can see that all CA-dots are brighter than quantum dots of similar spectrum. This puts CA-dots in the category of ultrabright fluorescent nanoparticles [18]. Notably functionalized water-dispersible QDs have typically smaller diameters of 15–30 nm [10]. One might expect that assembling several quantum dots together, one could get nanoparticles of larger size, and expectedly, higher brightness. However, it is impractical because quantum dots quench their fluorescence when the distance between them is less than ~10 nm [13,38]. Fig. 1d shows a fluorescent image of individual CA-dots in the vicinity of a glass slide imaged with 100× (1.4 N. A.) objective. The different fluorescent intensity of CA-dots can partially be explained by out-of-focus of some particles and particle aggregation on the glass surface.

The particle fluorescence displays much better photostability compared to the free dye (Fig. 1f). As expected, the photostability of dye molecules substantially improves after encapsulation since the polymer matrix limits the availability of oxygen species to initiate bleaching and decreases the thermal motion of dye molecules. For each dye, dramatic improvement in photodegradation resistance is observed after nearly 10 min of irradiation. The encapsulated green and yellow dyes, in particular, exhibit essentially zero degradation while their corresponding free dyes diminished in intensity by 8% and 2%, respectively.

The surface coating of CA-dots can be indirectly verified using the Zeta-potential measurements. Native cellulose acetate particles are negatively charged due to the outward orientation of hydroxyl groups produced during self-assembly (Zeta potential is ~30 mV in neutral pH). The assembly of CA-dots coated with PEG and PEG-FA noticeably mitigates negative surface potentials of CA-dots (Table 1). It should be noted that still negative overall Zeta potential is important for in vivo applications to avoid fast removal of the particles from blood circulation [39].

To estimate the amount of folate molecules per nanoparticles, we use Raman and absorbance spectroscopy. Decomposing the relative contribution from different constituents of the particles, we can estimate the total amount of folate molecules per particle, Table 1 (see Ref. 32 for detail). It should be noted that it is the estimation of the bulk value of folate molecules, not only those which are located on the surface. Therefore, this estimation should be evaluated as an upper bound estimate for the number of folate molecules on the surface.

CA-dots for IV-injection in vivo

To demonstrate intravenous (IV) application of CA-dots particles in vivo, we utilized human cervical epithelial cancer xenograft model in zebrafish. Since the majority of epithelial cancer cells overexpress folic acid receptors, folate-functionalized CA-dots should preferentially target epithelial tumors within zebrafish. The tumors were initiated through the injection of human cervical epithelial (HeLa) cells near the fish eye (see Fig. 2 of Ref. 32). After xenografting, the cancer cells began to spread and create metastases. The fish was immobilized in agarose gel and imaged using a long working distance fluorescent microscope (see Ref. 32

Please cite this article in press as: B. Peng et al., Materials Today (2018), https://doi.org/10.1016/j.mattod.2018.11.001

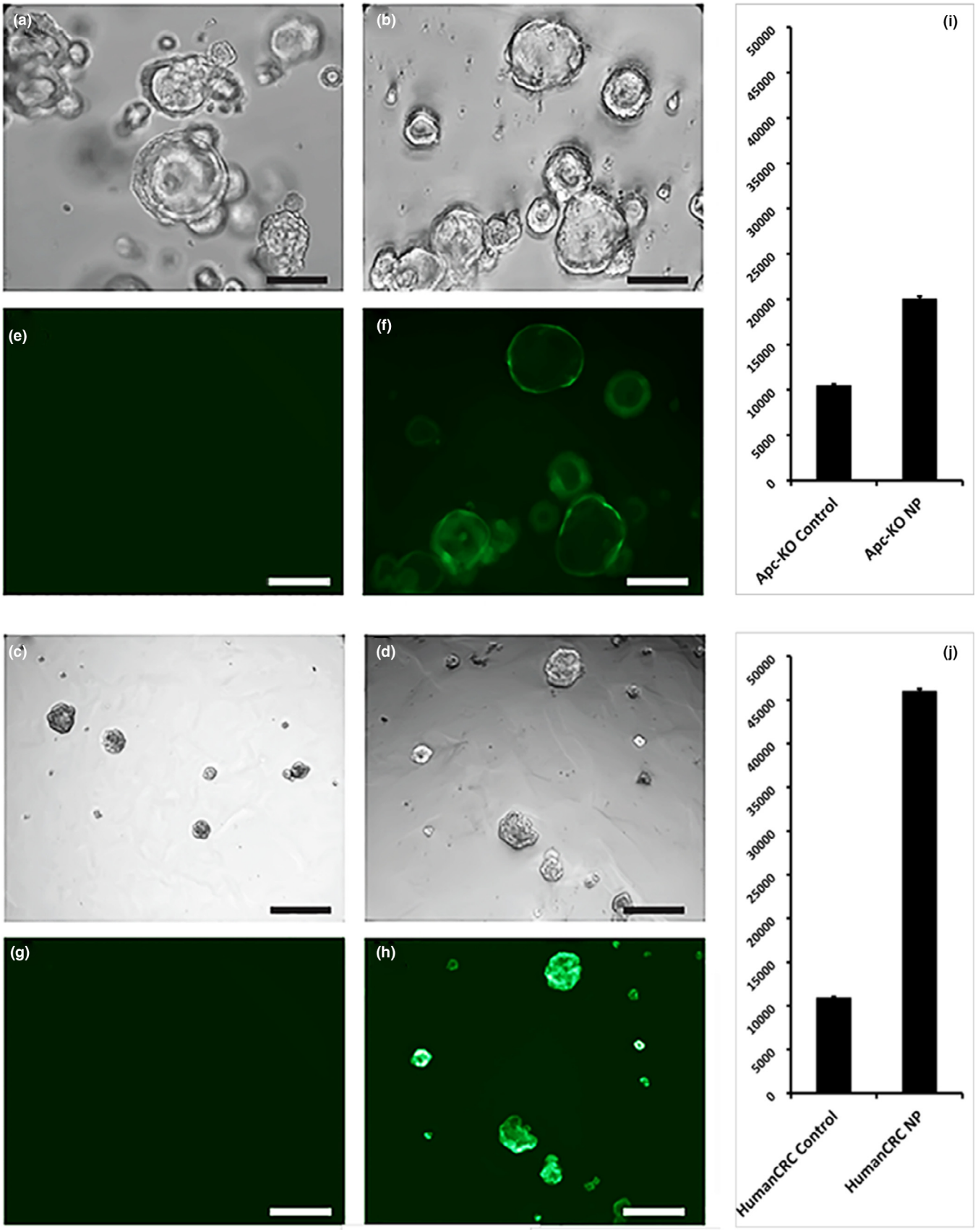

FIGURE 4

Apc-knockout mouse colon organoids (A, B, E, F) and human colorectal cancer (CRC) organoids (C, D, G, H) incubated in control nanoparticles (A, E, C, G) and functionalized nanoparticles (B, F, D, H) under brightfield microscopy and fluorescent microscopy. Scale bar is 100 μm. Mean fluorescent intensity (MFI) of (I) Apc-knockout mouse colon and (J) human CRC organoids incubated in control nanoparticles and folate-conjugated nanoparticles.

Please cite this article in press as: B. Peng et al., Materials Today (2018), https://doi.org/10.1016/j.mattod.2018.11.001

for detail). HeLa cells were modified to overexpress RFP (from PDONR221-RFP in lentiviral system) for the ease of identification. We choose CA-SB-PEG-FA nanoparticles which fluorescence in the blue region, which is not overlapping with RFP. This enables straightforward quantification of colocalization of particles with cancer cells, and thus, evaluation of targeting efficiency. CA-SB-PEG particles served as a material control, with the strategy of achieving contrast within tumors by passive diffusion or EPR (Enhanced Permeability and Retention) and not by the active targeting [43].

Very good co-localization between tumors and folate-functionalized CA-dots is observed even after 30 (Fig. 3 of Ref. 32). After 50 min, it reaches high accuracy of tumor detection (Fig. 2a–c), resulting in a sensitivity (i.e., accuracy of detection of tumor) of 96%, a specificity (i.e, accuracy of detection of absence of tumor) of 96%, and an accuracy (the percentage of correct identification of both tumor and absence of tumor) of 96%. Although we see some nonspecific targeting using control CA-dots (Fig. 2d–f) due to leaky vasculature [43] of tumors, much less accumulation of the control particles within tumors was observed (a sensitivity of 65%, a specificity of 80%, and an accuracy of 76% were observed, see Ref. 32 for detail). This proves specific folate functionalization of CA-dots as well as their capability the target tumors in vivo.

It is interesting to note that one can clearly identify tumors as small as 10 μm. Since imaging was performed within 30 min after injection, the detected size is ~37× smaller and the detection time ~6× faster compared to the previous art (though it was attained on rats: 370 micron and submillimeter-sized tumors were observed after intraperitoneal injection [44,45], respectively). Early detection of small tumors is significant from both applied and fundamental point of use. Clinical outcomes improve and patient mortality significantly decreases when surgeons can recognize and remove submillimeter tumors [44]. It is worth noting that the fluorescent images presented in this work were obtained using a long working distance (Olympus MVX-10) stereo microscope, which could directly be used in real surgery. It is definitely interesting to follow the fate of the particles after the observed targeting. This will require long-term study of biodistribution, which we plan to do in future works. It is worth noting that we do not expect toxicity due to possible biodegradation of cellulose acetate, which is a potential problem for some biodegradable particles, for example made of PLGA [46]. Cellulose acetate is not biodegradable at least in human organism [47].

CA-dots for topical tumor targeting ex vivo

Another challenging application for targeting is specific labeling of tumors via topical application of targeting particles. Here we demonstrate targeting ability of folate functionalized CA-dots using an ex vivo model of colorectal cancer in *Villin*^{CreERT2}-*Apc*$^{fl/fl}$ mice. Tumors were studied four weeks status post multiple 4-hydroxy-tamoxifen mucosal injection into the distal colon. After euthanizing, the mouse colon was extracted, gently washed with PBS, and cut with scissors (Fig. 3a,c,f). PBS solution of 0.1 mg/mL of green CA-dots (CA-GREEN-PEG-FA) was introduced on the freshly open colon. After 10 min of incubation, the colon was gently rinsed, placed in clear PBS solution and photographed with a long focus fluorescent microscope (Fig. 3b–f). One can clearly see green fluorescence coming from the locations of tumors, which are easy to identify targeting on brightfield photographs (Fig. 3a,c,f). Normal parts of colon do not show a noticeable targeting (Fig. 3b,d,f). It is interesting to note rather high heterogeneity of tumor labeling by folate functionalized CA-dots (Fig. 3f). This presumably comes from the heterogeneity of folate receptors on the surface of cancer cells.

To verify if folate functionalized CA-dots are specific to colorectal cancer cells, the targeting was also verified on specially prepared organoids or "mini-intestines" that are deficient in the Apc tumor suppressor gene (similar to cancer studied above). Apc-knockout colon mouse organoids and human colorectal cancer organoids were incubated for 10 min at 37 °C with folate-conjugated nanoparticles and non-functionalized nanoparticles as the control. Bright-field and fluorescent microscopy pictures were obtained as illustrated by Fig. 4. We observed significantly increased fluorescence in organoids incubated in folate-conjugated nanoparticles. Mean fluorescent intensities were calculated and demonstrated a significant difference between both groups ($P < 0.0001$). This implies that folate-mediated mechanism of specific targeting of colon tumors is a plausible hypothesis of the observed cancer-specific contrast.

Conclusion

We have developed a platform to synthesize novel bright fluorescent nanoparticles using one of the cellulose derivatives, cellulose acetate. The developed approach is modular. It consists of synthesizing conjugates of various copolymer – biomolecules of interest (ligand), and then using one of those conjugates for supramolecular assembly of CA-dots. Commercial fluorescent dyes can be used without any modifications to create fluorescent properties of CA-dots. Because the fluorescent dye should be initially dissolved in the organic solvent together with cellulose acetate, a broader class of hydrophobic fluorescent dyes can also be used. Further, it is possible to use a physical mix of different dyes within each particle. As a result, a large number of fluorescent spectra can be attained. In principle, the strategy is not limited to encapsulating only fluorescent molecules. Various active (bio)materials can be encapsulated inside CA-dots in a similar manner. It may include different drugs and their combinations for therapeutic and theranostic applications. Excellent targeting of epithelial tumors demonstrated here makes the application of these particles quite promising.

Materials and methods

Materials

30-K molecular weight cellulose acetate and Pluronic F127 (PF127) was purchased from Sigma-Aldrich (St. Louis, MO). Dimethylsulfoxide (DMSO) and acetone were purchased from ThermoFisher Scientific (Waltham, MA) and Sigma-Aldrich (St. Louis, MO), respectively. Carboxydiimidazole was purchased from Sigma-Aldrich (St. Louis, MO). 12 kD dialysis membranes were obtained from Spectrum Labs (Waltham, MA). 450-nm pore size Acrodisc syringe filters were obtained from Pall Corp (Port Washington, NY). The fluorescent dye, Stilbene 420, was obtained from Exciton, Inc. (Dayton, OH).

Please cite this article in press as: B. Peng et al., Materials Today (2018), https://doi.org/10.1016/j.mattod.2018.11.001

Synthesis of supramolecular cellulose acetate nanoparticles

A 1 mg/mL cellulose acetate (CA) solution was prepared 30 K MW CA (Sigma-Aldrich) in organic solvent – DMSO/THF/acetone—(Fisher Scientific, Sigma-Aldrich) via stirring and sonication at room temperature for 3 h. Separately, a water-soluble guest polymer, PF-127 (Sigma-Aldrich) is stirred into DI water (final polymer concentration of 0.49 mg/mL) over 2 h. The CA solution is introduced into the aqueous guest polymer solution under high agitation to facilitate nanoparticle assembly. The combined solution was allowed to stir for 12 h at room temperature. Solvent removal was initiated by placing the mixture under vacuum at 50 C. Trace solvent was removed by dialyzing the nanoparticle solution for 4 days with dialysate changing every 3 h for the first 2 days (6 h for nights) and every 12 h thereafter. Large particulates are removed with a 450-nm pore size syringe filter (Pall Acrodisc).

Synthesis of control (PEG coated) and targeted (PEG-folate) cellulose acetate nanoparticles

A 1 mg/mL cellulose acetate (CA) solution was prepared by dissolving 2 mg of 30 K MW CA (Sigma-Aldrich) in a 2 mL of DMSO/acetone (15:85 v/v) mixture (Fisher Scientific, Sigma-Aldrich) via stirring and sonication at room temperature for 3 h. The dyes were introduced as described in the following example. 1 mg of Stilbene 420 (Exciton, Inc) was dissolved by introducing to the CA solution and stirred at room temperature for 30 min. Separately, for targeted particles, 50 μL of (concentration 10 mg/mL) PF-127-FA conjugated polymer solution was stirred into DI water (final polymer concentration of 0.49 mg/ml) over 10 min. Preparation of Pluronic F127-folic acid conjugated polymer is described in Ref. 32). The CA solution with Stilbene 420 is quickly introduced into the PF-127-FA aqueous solution under high agitation to facilitate nanoparticle assembly. For control, PEGylated particles with no targeting ligand, 65 wt% of PF-127 polymer in water was prepared by stirring over 2 h. The resulting CA solution with Stilbene 420 is introduced into the PF-127 aqueous solution. In both control and targeted CA particle syntheses, the combined organic-aqueous solution was allowed to stir for 12 h at room temperature. The solvent was removed by placing the mixture under vacuum at 50 C. Trace solvent and free dye were removed by dialyzing the nanoparticle solution for 4 days with dialysate changing every 3 h (6 h at night) for the first 2 days and every 12 h thereafter. Dialysis is complete when no fluorescence of non-encapsulated Stilbene 420 is present in the dialysate. Large particulates are removed with a 450-nm pore size syringe filter (Pall Acrodisc).

Dynamic light scattering

Dynamic Light Scattering (DLS) and zeta-potential measurements were conducted in DI water on a Malvern Zetasizer Nano ZS instrument after equilibration at 25C. The intensity-average size (Z-average) and most probable size (mean of number weighted distribution) was the average of three measurements. Typically, DLS uses the laser light of 633 nm and the backscattered light is monitored over light at an angle of 173°. 0.1 mg/mL nanoparticle concentration was used for both size and zeta potential measurements in DI water.

Atomic force microscopy

Bioscope Catalyst (Bruker/Veeco, Inc., Santa Barbara, CA) atomic force microscope equipped with a Nanoscope V controller was used in the study. Standard AFM cantilever holders for operation in air were employed. The particles were immobilized on glass slides prepared as follows. Glass slides were placed in an ethanol bath and sonicated for 15 min in order to cleanse the surface. Following washing, slides were dried under forced nitrogen gas. Poly-l-Lysine coating was applied to the glass slides via a standard Sigma-Aldrich protocol. In short, the 0.1% w/v poly-l-Lysine solution was diluted 1:10 with deionized water. This working solution was stored in a refrigerator at 2–8 °C and allowed to come to room temperature when used. Glass slides were incubated in the poly-l-Lysine solution for 5 min, drained and washed with DI water, and dried overnight at room temperature. Then a drop of 0.1 mg/mL solution of nanoparticles was dispensed on the slide and incubated for 60 min to allow electrostatic attachment of negatively charged particles to the positively charged glass surface. AFM imaging was performed once slides were washed and dried.

Measurements of fluorescent properties

Particle fluorescence, brightness, and photostability were measured using the FLUOLOG 3 fluorimeter by Horiba and a UV–VIS Cary 60 spectrophotometer by Agilent. To characterize fluorescent brightness of nanoparticles, we follow the basic definition of the brightness of fluorophores used in flow cytometry, MESF units (Molecules of Equivalent Soluble Fluorophore). This definition is based on the comparison brightness of nanoparticles and a fluorophore of known brightness within the same spectral range (reference fluorophore). Such a definition is independent of a particular spectrometer or methods of measurement. The brightness of a single nanoparticle was calculated using the following formula:

$$\text{Brightness [MESF units]} = (FL_{NP}/C_{NP})/(FL_{dye}/C_{dye}), \quad (1)$$

where FL_{NP} or FL_{dye} is the fluorescence intensity of a nanoparticle suspension or reference dye solution, respectively. The spectra of both CA nanoparticles and the reference dye solution are very close, so the fluorescence units measured from each sample was evaluated by integrating over the same emission wavelength interval [18,48]. The exact intervals and relative brightness obtained in the measurements are shown in Table 1 of Ref. 32.

Photostability measurements

Photostability measurements were performed by illuminating 3 mL of fluorescent nanoparticle solutions of the same optical density of 0.01 with white light of 450 W xenon lamp while monitoring intensity with a Horiba Fluorolog 3 (Horiba, Japan) fluorimeter. Optical densities of fluorescent free dye and particles were chosen to have the same 0.01 absorbance. The solutions were separately irradiated continuously using the white light source using a slit width of 14.7 nm. (For comparison, a 1 nm slit width was used when doing standard fluorescence measurements.) Initial fluorescence intensity was recorded at time zero and represents the maximum intensity. Fluorescence was recorded every 60 s following continuous exposure and normalized by the maximum intensity to produce a measure of %

Please cite this article in press as: B. Peng et al., Materials Today (2018), https://doi.org/10.1016/j.mattod.2018.11.001

fluorescence remaining. Photostability measurements were performed for 10 min or in the linear kinetic range of photodegradation (up to 80–90% of the initial fluorescence).

In vivo imaging of cellulose acetate nanoparticles in zebrafish

Hela cells overexpressing RFP (from pLenti-III-RFP-N in lentiviral system) were grown up to 70% confluency in DMEM medium with 10% FBS at 37 °C and 5% CO_2. Hela-RFP cells were harvested using Trypsin, washed 3 times, counted and resuspended in full growth medium at a final concentration of 50×10^6 cells per mL.

All animals were handled as described in the Boston University School of Medicine zebrafish facility, in accordance with our IACUC-approved protocol. AB zebrafish were bred and embryos were raised in the dark up to 2 days post fertilization (dpf). The 2 dpf zebrafish larvae were anesthetized with Tricaine and immobilized for Hela-RFP cell microinjection using sharpened borosilicate glass capillaries (1.0 mm O.D. × 0.78 mm). The Hela-RFP cell micro-injections were all performed by injection of ~1 nL directly into the periviteline cavity of the embryo using a micro-injection station. Zebrafish embryos were then incubated for 20–28 h in the dark at 35 °C to allow cancer cell spreading to occur.

After Hela-RFP cells widely spread (3 dpf), embryos with evident metastasis were delicately embedded in 3% low melting temperature agarose gel and micro-injected directly behind the eye with ~0.5 nL of 1 mg/mL particles CA-dot solutions for time courses and imaged using an Olympus MVX-10 microscope. The measurements of tumor – particle co-localization, calculation of sensitivity, specificity, and accuracy are described in detail in Ref. 32.

Mouse colon

Colonic tumors were achieved using a previously described *in vivo* murine model for colon cancer [49]. Briefly, mice with $Apc^{fl/fl}$-$Villin^{CreER}$ genetic background underwent colonoscopy-guided colonic mucosal injections of 4-hydroxytamoxifen to perform *in situ* Apc deletion. Two weeks after the injection, colonoscopy of the mice showed tumor formation at the site of injection. Then, the mice were sacrificed, and the colon was dissected and isolated. The colon was cut along its longitudinal axis, was washed gently with cold PBS on ice, and placed on a transparent sterile petri dish. Experiments by application of different nanoparticles were performed under those conditions, and pictures were taken under a fluorescent dissecting microscope.

Colon mouse and human organoids

The colon mouse organoids were prepared and cultured and genetically modified to produced Apc-knockouts by a previously described method [50,51]. Briefly, $Apc^{fl/fl}$-$Villin^{CreER}$ mice were sacrificed and the colon was dissected and isolated. After incubation in ethylenediaminetetraacetic acid (EDTA), the colonic crypts were scrapped off using a glass slide, collected in PBS, and then spun down. The crypts were mixed with matrigel at an appropriate concentration (i.e. 4–10 crypts/μL), and 50 μL of the mixture was plated in the center of a 24-well plate. After allowing 10 min for matrigel to polymerize at 37 °C, 500 μL of appropriate culture media consisting of Advanced Dulbecco's Modified Eagle Medium (ADMEM), Wnt3a, R-spondin, and Noggin, were added to the well. 4-hydroxytamoxifen at a final concentration of 20 nM was added to the surrounding media. The organoids were incubated at 37 °C and 4% carbon dioxide condition for 2 days and allowed to form organoids. The media were then changed to minimal media that lack Wnt3a, R-spondin and Noggin, to allow for selection of Apc-knockout organoids.

Acknowledgments

NSF support (grant CBET 1745530) is gratefully acknowledged by I.S. H.F. acknowledges support from NIH (grant CA215059) and the St. Baldrick's Foundation. F.J.F.L. acknowledges fellowship from Boston University Innovation Center-BUnano Cross-Disciplinary Training in Nanotechnology for Cancer (XTNC).

Author contributions

B.P. and I.S. conceptualized and designed methods and experiments related to assembly of CA-dots. B.P. performed the particle synthesis and characterization. S.P. developed method for bioconjugation to the guest polymer. M.E.D. did the AFM measurements of the particle sizes. J.R., I.S., M.A. and O.H.Y. designed the experiments on colorectal mouse cancer. M.A. and B.P. conducted the mouse tumor targeting experiments. M.A. designed and performed the experiments with colon organoids. H.F. and F.J.F.L. designed the experiments with zebrafish. F.J.F.L. conducted the zebrafish experiments. B.P. calculated the statistics of targeting in zebrafish. I.S. and B.P. wrote the manuscript. All authors discussed the manuscript.

Competing financial interests

P.B. and I.S. are co-inventors on the US pending patent App. 15/363,077 "Functionalized nanoparticles with encapsulated cargo and method of their self-assembly" filed by NanoScience Solutions, LLC. The other authors declare no competing financial interests.

Data availability

Data will be made available on request. Some data cannot be shared at this time due to technical or time limitations-the data also form part of an ongoing study. Additional data related to the topic of this paper can be found in [52].

References

[1] B. Yang et al., Mater. Today 19 (5) (2016) 284.
[2] L. Shang, G.U. Nienhaus, Mater. Today 16 (3) (2013) 58.
[3] P.S. Eastman et al., Nano Lett. 6 (5) (2006) 1059.
[4] M.J. Fritzler, Lupus 15 (7) (2006) 422.
[5] X.H. Gao, S.R. Dave, Bio-Appl. Nanopart. 620 (2007) 57.
[6] J.V. Jokerst et al., Biosens. Bioelectron. 24 (12) (2009) 3622.
[7] L. Wang, W. Tan, Nano Lett. 6 (1) (2006) 84.
[8] L. Wang et al., Bioconjug. Chem. 18 (2) (2007) 297.
[9] J. Gao et al., Small 6 (2) (2010) 256.
[10] X. Gao et al., Nat. Biotechnol. 22 (8) (2004) 969.
[11] I.L. Medintz et al., Nat. Mater. 4 (6) (2005) 435.
[12] D. Bimberg, U.W. Pohl, Mater. Today 14 (9) (2011) 388.
[13] U. Resch-Genger et al., Nat. Methods 9 (2008) 763.
[14] Y.H. Chan et al., Anal. Chem. 84 (21) (2012) 9431.
[15] Y.H. Jin et al., ACS Nano 5 (2) (2011) 1468.
[16] C. Wu et al., J. Am. Chem. Soc. 132 (43) (2010) 15410.
[17] E.Y. Ye et al., Mater. Today 17 (4) (2014) 194.
[18] V. Kalaparthi et al., J. Mater. Chem. C 4 (11) (2016) 2197.

Please cite this article in press as: B. Peng et al., Materials Today (2018), https://doi.org/10.1016/j.mattod.2018.11.001

[19] E.N. Bifari et al., Curr. Pharm. Des. 22 (20) (2016) 3007.
[20] F.J. Pavinatto et al., Biosens. Bioelectron. 67 (2015) 553.
[21] K. Ng et al., Mater. Today 20 (1) (2017) 32.
[22] S. Anitha et al., Carbohyd. Polym. 97 (2) (2013) 856.
[23] L. Sacarescu et al., Cellulose 23 (6) (2016) 3847.
[24] P. Trivedi et al., Cellulose 23 (3) (2016) 1751.
[25] M.R. Kulterer et al., Adv. Funct. Mater. 22 (8) (2012) 1749.
[26] J.V. Jokerst et al., Nanomedicine (Lond) 6 (4) (2011) 715.
[27] E. Blanco et al., Nat. Biotechnol. 33 (9) (2015) 941.
[28] C.P. Leamon, P.S. Low, PNAS 88 (13) (1991) 5572.
[29] S. Hornig, T. Heinze, Biomacromolecules 9 (5) (2008) 1487.
[30] H. Fessi et al., Int. J. Pharm. 55 (1) (1989) R1.
[31] B. Lindman et al., J. Mol. Liq. 156 (1) (2010) 76.
[32] P.H. Wu et al., Nat. Methods 15 (7) (2018) 491.
[33] G. Mattson et al., Mol. Biol. Rep. 17 (3) (1993) 167.
[34] W.C.W. Chan et al., Curr. Opin. Biotechnol. 13 (1) (2002) 40.
[35] W.C.W. Chan, S.M. Nie, Science 281 (5385) (1998) 2016.
[36] J. Lei et al., ACS Nano 5 (5) (2011) 3447.
[37] S. Palantavida et al., J. Mater. Chem. B 2 (20) (2014) 3107.
[38] M. Dokukin et al., Appl. Phys. Lett. 95 (17) (2009) 173105.
[39] M.J. Adams et al., Arch. Virol. 160 (7) (2015) 1837.
[40] U. Resch-Genger et al., Nat. Methods 5 (9) (2008) 763.
[41] Y. Wu et al., Anal. Biochem. 364 (2) (2007) 193.
[42] Y.H. Chan et al., J. Am. Chem. Soc. 134 (17) (2012) 7309.
[43] Y. Matsumura, H. Maeda, Cancer Res. 46 (12 Pt 1) (1986) 6387.
[44] A.H. Colby et al., ACS Nano 11 (2) (2017) 1466.
[45] A. Oseledchyk et al., ACS Nano (2016).
[46] J. Cheng et al., Biomaterials 28 (5) (2007) 869.
[47] J. Puls et al., J. Polym. Environ. 19 (1) (2011) 152.
[48] E.B. Cho et al., Small 6 (20) (2010) 2314.
[49] J. Roper et al., Nat. Protoc. 13 (2) (2018) 217.
[50] K.P. O'Rourke et al., Bio Protoc 6 (2016) 4.
[51] J. Roper et al., Nat. Biotechnol. 35 (6) (2017) 569.
[52] B. Peng et al., Data in Brief, in press. https://doi.org/10.1016/j.dib.2018.12.030

Please cite this article in press as: B. Peng et al., Materials Today (2018), https://doi.org/10.1016/j.mattod.2018.11.001